EurJIC
European Journal of Inorganic Chemistry

Full Paper
doi.org/10.1002/ejic.202000433

Rhenium Radiofluorination

Telescoping the Synthesis of the [^{18}F]CABS13 Alzheimer's Disease Radiopharmaceutical via Flow Microfluidic Rhenium(I) Complexations

Mitchell A. Klenner,*[a,b] Benjamin H. Fraser,[a] Vaughan Moon,[a,c] Brendan J. Evans,[a,c] Massimiliano Massi,[b] and Giancarlo Pascali*[a,d,e]

Abstract: The syntheses of rhenium(I) complexes were achieved under flow microfluidic conditions. The use of a single microreactor was applied towards complexation of the 6-chloro-2,2′-bipyridine diimine ligand, with ideal complexation conditions around 170 °C. Subsequent radiolabelling with [^{18}F]fluoride was further achieved by flowing through a second heated microreactor, alongside a stream of dried radiofluorination media. Temperature modulation across both microreactors resulted in 23.6 % and 37.0 % radiochemical yield (RCY) of [^{18}F]6-fluoro-2,2′-bipyridine and its associated [^{18}F]tricarbonyl-(2-fluoro-2,2′-bipyridine)rhenium(I) chloride complex, respectively. Translation of this set-up to the synthesis of the [^{18}F]CABS13 Alzheimer's disease positron emission tomography (PET) imaging agent was achieved with the incorporation of a third microreactor to enable thermal control of the complexation, fluorination and decomplexation pathways. Optimal RCYs of 2.7 % and 1.9 % of [^{18}F]CABS13 and its rhenium(I) complexation were achieved in-flow, respectively. However, discrepancies in the RCYs were found to arise from differences in the grade of anhydrous dimethyl sulfoxide (DMSO) employed in the continuous-flow reactions. Anhydrous DMSO from Sigma-Aldrich (≤ 99.9 %) in former experiments afforded higher yielders in comparison to replicate experiments employing anhydrous DMSO from Merck Millipore (≤ 99.7 %), thus demonstrating that control of the solvent grade is key to optimizing reaction RCYs.

1. Introduction

Alzheimer's disease (AD) is currently the sixth leading cause of death in the United States, and the cause of 60–70 % of dementia cases.[1] The rate of cases is projected to increase, with a 2016 report from the Alzheimer's Association claiming that a new person develops the neurodegenerative disease every 66 seconds.[2] These cases have amounted to an estimated 5.8 million Americans living with AD, as of 2019, with $290 billion in payments being made for the long-term health care and hospice services of ≥ 65 year-old patients suffering from dementia in the same year.[3] Many efforts have hence been undertaken to elucidate the mechanisms underlying AD and to develop diagnostic agents for early interventional treatment. Two prevalent characteristics of AD, exempting genetic factors, are neurofibrillary tangles (NFTs) formed from the hyperphosphorylation of tau proteins within the neurons which lead to cytoskeletal collapse alongside malfunctions in neurotransmission,[4] and amyloid beta (Aβ) plaques which form from entangled oligomers and disrupt synaptic networks.[5] Concerning the latter characteristic, Vasdev, et al. developed a PET radiopharmaceutical, 2-[^{18}F]fluoro-8-hydroxyquinoline ([^{18}F]CABS13), for the in vivo imaging of Aβ plaques.[6] The tracer, [^{18}F]CABS13, takes into account that Zn, Cu and Fe ions are involved in Aβ plaque deposition and stabilization,[7] and that metal chelating agents can facilitate dissolution of Aβ deposits by preventing metal–Aβ interactions,[8] thereby presenting both therapeutic and diagnostic strategies for AD and related dementias. The radiopharmaceutical was first administered to an amyloid precursor protein and presenilin-1 (APP/PSEN1) transgenic mouse model of AD, which exhibited a significant temporal difference in both brain uptake and retention compared with the wild-type control model.[6] PET neuroimaging in non-human primate models of AD, however, demonstrated comparatively low brain uptake and rapid in vivo metabolism of the tracer.[9] The vast discrepancies in pharmacokinetic behavior between the species have prolonged investigations concerning the efficacy of the radio-

[a] Dr. M. A. Klenner, Dr. B. H. Fraser, V. Moon, B. J. Evans, Prof. G. Pascali
National Deuteration Facility (NDF) & Human Health, Australian Nuclear Science and Technology Organisation (ANSTO),
2234 Lucas Heights, NSW. Australia
E-mail: mitchk@antsto.gov.au
g.pascali@unsw.edu.au
[b] Dr. M. A. Klenner, Prof. M. Massi
School of Molecular and Life Sciences, Curtin University,
6102 Bentley, WA. Australia
[c] V. Moon, B. J. Evans
Department of Molecular Sciences, Macquarie University,
2109 Macquarie Park, NSW. Australia
[d] Prof. G. Pascali
Prince of Wales Hospital,
2031 Randwick, NSW. Australia
[e] Dr. G. Pascali
School of Chemistry, University of New South Wales (UNSW),
2052 Kensington, NSW. Australia
Supporting information and ORCID(s) from the author(s) for this article are available on the WWW under https://doi.org/10.1002/ejic.202000433.
Part of the Special Collection for the 44th ICCC Conferences.

Full Paper
doi.org/10.1002/ejic.202000433

tracer for PET diagnoses of AD in humans, particularly in light of nuclear medicines such as carbon-11 labelled Pittsburgh Compound B ([^{11}C]PiB) currently being trialed for diagnoses of human cerebral Aβ pathologies.[10] However, alternative hydroxyquinoline-based treatments for neurodegeneration such as 5-chloro-7-iodo-8-hydroxyquinoline (clioquinol, CQ), have demonstrably reversed the in vivo progression of AD and resulted in rapid restoration of cognitive ability in APP transgenic mouse models.[11] Notably, CQ also outcompetes APP derived oligomers for metal ions without affecting the activity of Zn/Cu-dependent enzymes,[11,12] thus warranting continued study of hydroxyquinoline radiopharmaceutical analogues. Towards furthering the investigation of [^{18}F]CABS13 as an AD imaging agent, a few radiosynthetic pathways have been described in literature. Each pathway has been characterized by multiple-step radiosyntheses involving radiofluorination of an alcohol-protected precursor, using benzyl or benzyloxymethyl protecting groups, followed by deprotection of the radiolabelled agent, either by acid-catalyzed hydrolysis or Pd/C-catalyzed hydrogenation.[6,9,13] One recent such method, which we reported in a 2020 study, utilized a rhenium(I) complexation-dissociation approach to enable radiofluorination of N-heterocyclic bidentate ligands which were unable to be radiosynthesised hitherto.[14] A mechanism was posited, based on density functional theory (DFT) modelling analyses, which involved fluorination of the *cis*-carbonyl ligand, thus forming an acyl [^{18}F]fluoride intermediate in proximity to the leaving group and facilitating nucleophilic aromatic substitution (S_NAr). In the case of hydroxyquinoline ligands, the rhenium(I) centre formed dative bonds with the N and O atoms, serving as both an activator for S_NAr and a protecting group for the alcohol simultaneously. This experiment incorporated only a single microreactor, however, which provided limited control over the thermally mediated radiofluorination and decomplexation processes. As a means of simplifying the radiosynthesis of [^{18}F]CABS13 to a single radiosynthetic reaction, we have sought to couple our rhenium(I) complexation-dissociation approach[14,15] with a multiple microreactor in-flow microfluidic set-up hypothesized to enable thermal control of the fluorination and dissociation conditions. Only one other two-step telescoping radiotracer production method has been reported, which expedited syntheses of [^{18}F]fluorocholine derivatives.[16] Complexation of the precursor ligand to a source of rhenium(I) was also trialed in-flow, both for CABS13 and a chloro-substituted bipyridine compound, to spare the additional step of synthesis typically required to prepare the rhenium(I) precursor. Such a method accompanies the few literature examples describing automated multiple step in-flow syntheses of fluorine-18 labelled PET radiopharmaceuticals.[17] However, by telescoping such radiosyntheses, ensuring that the first reaction does not negatively interfere with the second, we present a rarely implemented strategy designed to reduce the burden on synthetic chemists tasked with preparing radiolabelling precursors. More significantly, this approach represents the first demonstration of in-flow rhenium(I) complexation, particularly as applied under microfluidic conditions, which may have far-reaching implications for the manufacturing of many similar rhenium(I) tricarbonyl tracers.

2. Results and Discussion

The precursors and non-radioactive standards were synthesized as per our previously published methodology via the scheme depicted in Figure 1.[14] 6-Chloro-2,2′-bipyridine (**6ClBiPy**) was first complexed to a source of pentacarbonylrhenium(I) chloride (**$Re(CO)_5Cl$**) in toluene solution to afford the tricarbonyl(6-chloro-2,2′-bipyridine)rhenium(I) chloride (**[$Re(6ClBiPy)(CO)_3Cl$]**) precursor. Starting material **6ClBiPy** was also fluorinated via S_NAr with potassium fluoride in dimethyl sulfoxide (DMSO) solution using 18-crown-6 ether as a phase-transfer catalyst (PTC) in azeotropically distilled anhydrous acetonitrile solution, which required four days of refluxing to afford the 6-fluoro-2,2′-bipyridine (**6FBiPy**) non-radioactive standard. The **6FBiPy** ligand was then complexed with **$Re(CO)_5Cl$** in toluene to afford the desired tricarbonyl(6-fluoro-2,2′-bipyridine)-rhenium(I) chloride (**[$Re(6FBiPy)(CO)_3Cl$]**) non-radioactive standard.

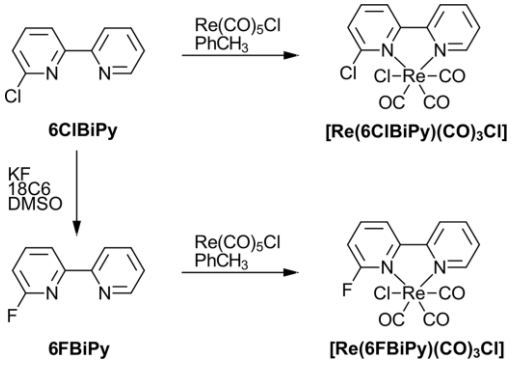

Figure 1. Synthetic route used to obtain the **6ClBiPy** and **[$Re(6ClBiPy)(CO)_3Cl$]** precursors, as well as the **6FBiPy** and **[$Re(6FBiPy)(CO)_3Cl$]** non-radioactive standards.

In-flow complexation was achieved via the microfluidic set-up assembled as per Figure 2. Here, the supply and flow rate of **6ClBiPy** in DMSO (0.74 mg mL^{-1}, 3.45 μmol mL^{-1}) solution was delivered by pump 1 (P1) from the relevant storage loop. The first 50 μL of the reagent was dispensed to a waste vial via backpressure created from aspirating and dispensing anhydrous DMSO solvent to ensure a uniform concentration of **6ClBiPy** in the reaction bolus. Reagent **$Re(CO)_5Cl$** in DMSO (1.36 mg mL^{-1}, 4.30 μmol mL^{-1}) was likewise aspirated and dispensed from a storage loop via pump 2 (P2). Volumetric ratios of 1:1 were applied for the precursor boluses, thus ensuring a 1.25 equiv. excess of **$Re(CO)_5Cl$** to **6ClBiPy** similar to the bulk synthesis. The reaction boluses (10 μL) of both reagents were eluted through microreactor 1 (MR1) with anhydrous DMSO at a 20 μL min^{-1} flow rate and eluted into the final product vial for analysis by high-performance liquid chromatography (HPLC). The internal volume of MR1 was 15.6 μL, which affords a residence time of approximately 23 s given the combined flow rate of 40 μL min^{-1} from both pumps. The temperature applied to MR1 was modulated in 20 °C increments via a heater plate to determine the optimal conditions for the complexation reaction. As the heat supplied to the reaction drive both the forward and reverse processes for complexation (K_c) and dissociation (K_{-d}), respectively, the temperature for maximal produc-

Full Paper
doi.org/10.1002/ejic.202000433

tion of **[Re(6FBiPy)(CO)$_3$Cl]** was hypothesized to lie between the two extremes of the 70–190 °C range trialed. Figure 3 depicts the 215 nm UV-absorbance channel for the resulting chromatograms at each of the tested temperatures. While the exact quantities of the products and unreacted starting materials are dependent on the molar absorptivity of each analyte at 215 nm, comparative assessments of production and consumption can be determined from the increase and decrease of the relative integrated peak areas, respectively. Evidently, higher temperatures resulted in increased production of the **[Re(6FBiPy)(CO)$_3$Cl]** complex, as quantified in Figure 4 which depicts the integrated peaks areas for each reagent expressed as a percentage of the entire chromatographic area at 215 nm alongside the associated standard deviations. The peak area of **Re(CO)$_5$Cl** notably decreases at temperatures greater than 90 °C and results in a considerable increase in the relative amount of **[Re(6FBiPy)(CO)$_3$Cl]** forming at 170 °C. At 190 °C the production of **[Re(6FBiPy)(CO)$_3$Cl]** is observed to decrease, suggesting that the increased heat supply favours the K_C rate constant up to 170 °C, whereafter the ratio of **[Re(6FBiPy)(CO)$_3$Cl]** complexation-to-dissociation rate decreases. An additional experiment was also employed at 190 °C, whereby the molar equivalence of **Re(CO)$_5$Cl** was scaled up two-fold (2.5 equiv.) to assess whether the rate of **[Re(6FBiPy)(CO)$_3$Cl]** complexation could be increased. The increased molar equivalence was the result of doubling the **Re(CO)$_5$Cl** solution bolus to 20 μL (i.e. by applying 1:2 volumetric ratio). This reaction is depicted by the dashed line of Figure 3, clearly indicating the retention time of **Re(CO)$_5$Cl** on the column and that excess reagent remained in the reaction media. Consequently, the **[Re(6FBiPy)(CO)$_3$Cl]** complex was afforded in a greater than two-fold increase in yield, as evidenced by Figure S1 of the SI which plots the integrated peak area with standard deviation, proportional to the relative mass of each reagent, for each compound at the given MR1 reaction temperature.

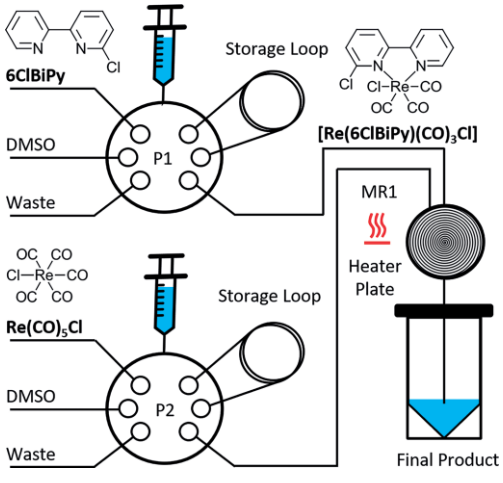

Figure 2. Microfluidic set-up for the automated syntheses of **[Re(6ClBiPy)(CO)$_3$Cl]** in-flow, used to determine the optimal temperature for complexation via heating of MR1.

After confirming that rhenium(I) ligand complexations could be achieved in-flow, we shifted our attention to the two-step radiosynthesis of [^{18}F]**6FBiPy** and [^{18}F]**[Re(6FBiPy)(CO)$_5$Cl** using an in-flow rhenium(I) complexation approach. The microfluidic set-up used to automate these reactions is illustrated in Figure 5. Solutions of **6ClBiPy** (1.47 mg mL^{-1}, 7.69 μmol mL^{-1}) and **Re(CO)$_5$Cl** (2.76 mg mL^{-1}, 7.69 μmol mL^{-1}) were still supplied by P1 and P2 in 10 μL boluses, respectively, and passed through heated MR1 to provide **[Re(6ClBiPy)(CO)$_5$Cl**. In this setup, a second microreactor (MR2) was placed in series to MR1 and temperature controlled to optimize the radiofluorination reaction. Cyclotron produced [^{18}F]fluoride in oxygen-18 enriched water, formed from the ^{18}O(p,n)^{18}F nuclear reaction, was eluted though a QMA ion exchange resin with tetraethylammonium (TEA) bicarbonate in a 90 % acetonitrile in water solution by pump 3 (P3). Adequate elution of [^{18}F]fluoride was confirmed by a decline in radioactivity, as measured by a γ-scintillation detector in close proximity, and a solenoid valve (SV) ensured the recycling of [^{18}O]water. The resulting TEA [^{18}F]Fluoride ([^{18}F]TEAF) solution was eluted into an azeotropic distillation vial, as confirmed by a nearby radioactivity detector, whereupon the solvent was evaporated under heated conditions with a nitrogen gas flow and vacuum applied through two SVs. The resulting residue was reconstituted with portions of anhydrous acetonitrile in order to azeotropically remove traces of water. The [^{18}F]TEAF complex was then finally reconstituted in anhydrous DMSO solution and transferred into a storage loop by pump 4 (P4). A fraction of the radioactive solution was dispensed into a waste vial to ensure homogeneity of the reaction bolus and 10 ± 2 MBq solutions of [^{18}F]TEAF were eluted through MR2 alongside the output of MR1 containing **[Re(6ClBiPy)(CO)$_5$Cl]**. Using the solution eluted from MR1 we aimed to telescope the synthesis of [^{18}F]**6FBiPy**, rather than its rhenium complexed analogue, by exploiting our previously described rhenium(I) complexation-dissociation approach. Thus, the temperature at MR2 was fixed at 190 °C in order to increase not only the rate of fluorination (K_f) forming [^{18}F]**[Re(6FBiPy)(CO)$_3$Cl]**, though also the rate of decomplexation (K_d) forming [^{18}F]**6FBiPy**. However, in this optimization, we again tested the variation of temperature of MR1 from 50–

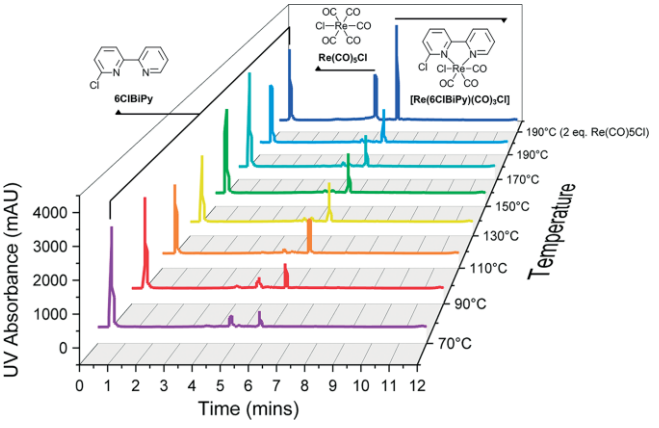

Figure 3. UV absorbance chromatograms showing the in-flow complexation of **6ClBiPy** with **Re(CO)$_5$Cl** to form **[Re(6ClBiPy)(CO)$_5$Cl** at varying temperatures. A two-fold equivalence of **Re(CO)$_5$Cl** was added in an additional 190 °C experiment to aid in driving the reaction. A gradient HPLC system of water and acetonitrile (5–95 %) was utilized with a flow rate of 2 mL min^{-1} and data collected at 215 nm wavelength.

Full Paper
doi.org/10.1002/ejic.202000433

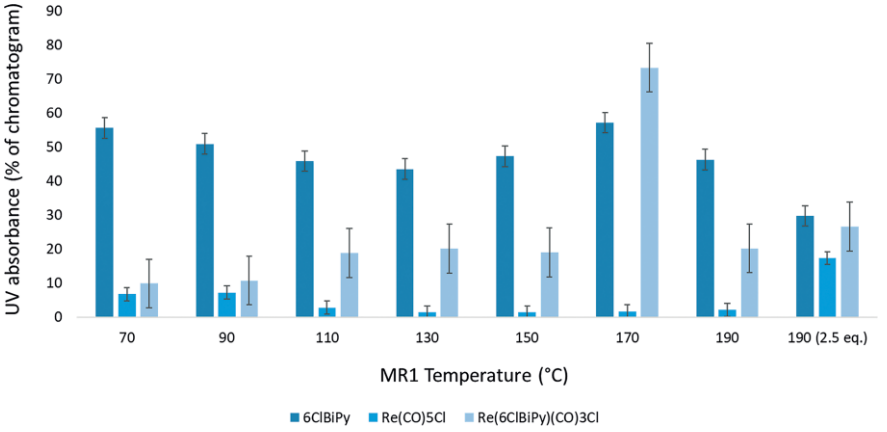

Figure 4. Relative percentage of integrated areas with associated standard deviations determined from the 215 nm UV-absorbance chromatograms for **6ClBiPy** and **Re(CO)$_5$Cl** complexation reactions forming **[Re(6ClBiPy)(CO)$_5$Cl** at varying MR1 temperatures.

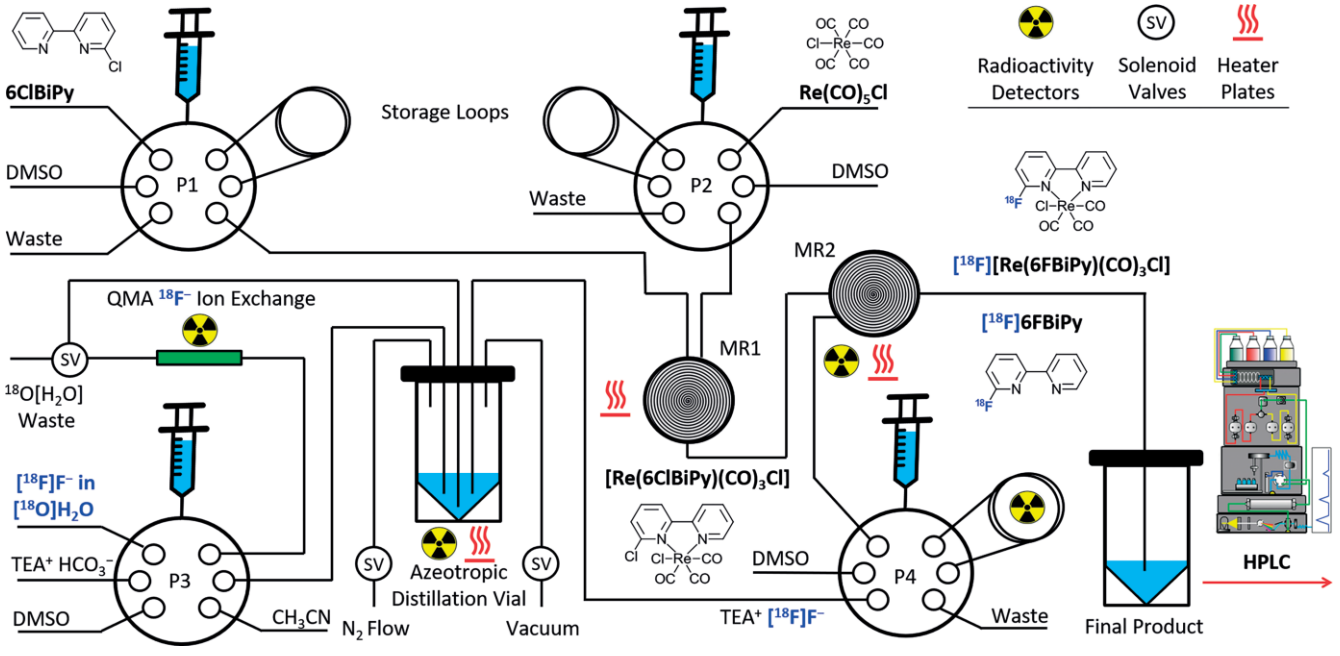

Figure 5. Microfluidic set-up for the complexation of **6ClBiPy** with Re(CO)$_5$Cl in MR1 to afford **[Re(6ClBiPy)(CO)$_3$Cl]**, followed by radiofluorination and decomplexation in MR2 to afford both [^{18}F]**[Re(6FBiPy)(CO)$_3$Cl]** and [^{18}F]**6FBiPy** radioproducts.

190 °C in 20 °C increments. The flow rates of P1 and P2 were both set to 10 μL min^{-1}, thus affording a combined flow of 20 μL min^{-1} through MR1. As the internal volume of MR1 was 15.6 μL, the residence time for the complexation reaction was thus approximately 47 s. P4 also dispensed the [^{18}F]TEAF solution at a rate of 10 μL min^{-1}, however MR2 consisted of a larger internal volume (31.2 μL) and thus a longer residence time of 62 s was allowed for the fluorination and decomplexation pathways despite a combined 30 μL min^{-1} flow rate. Additionally, a radioactivity detector was also placed in proximity of MR2 to monitor the elution of the radioactive solution into the final product vial for radioHPLC analysis.

The radiochemical yields (RCY), as determined from the integrated peak area of the radioproducts divided by the total radiochromatographic area, for both [^{18}F]**6FBiPy** and [^{18}F]**[Re(6FBiPy)(CO)$_3$Cl]**, are listed alongside the temperatures of MR1 and MR2 in Table 1. RCYs of less than 5 % were obtained for both radioproducts for an MR1 temperature of no greater

Table 1. RCYs of [^{18}F]**6FBiPy** and [^{18}F]**[Re(6FBiPy)(CO)$_3$Cl]** obtained from in-flow radiosyntheses applying MR1 (non-radioactive complexation) at the listed temperatures. MR2 (radiofluorination & dissociation) was also applied in-series at a fixed temperature of 190 °C.

MR1 Temperature [°C]	[^{18}F]6FBiPy (% RCY)	[^{18}F][Re(6FBiPy)(CO)$_3$Cl] (% RCY)
50	4.7	2.4
70	4.7	4.8
90	3.7	23.9
110	5.3	37.0
130	12.9	33.4
150	23.6	5.8
170	21.7	1.2
190	21.9	1.4

Full Paper
doi.org/10.1002/ejic.202000433

than 70 °C. At 90 °C, however, the radiosynthesis of [^{18}F]**[Re(6FBiPy)(CO)$_3$Cl]** was found to increase to 23.9 %, followed by maximum RCYs of 37.0 % and 33.4 % at 110 and 130 °C, respectively. Thereafter, the RCY of [^{18}F]**[Re(6FBiPy)(CO)$_3$Cl]** notably decreased as the complex dissociated to liberate [^{18}F]**6FBiPy** at a maximum of 23.6 % RCY at 150 °C, followed by consistent RCYs of 21.7 % and 21.9 % at 170 and 190 °C, respectively. As an example, the radiochromatogram acquired at 130 °C is depicted in Figure 6, which illustrates the retention of [^{18}F]**6FBiPy** at 2.15 min and [^{18}F][**Re(6FBiPy)(CO)$_3$Cl**] at 5.68 min, with minor radio by-products eluting around 4.5–5.0 min and unreacted [^{18}F]fluoride eluting around 30 s into the run. These radioactive by-products may possibly coincide with the minor by-products observed in the Figure 3 chromatograms for **[Re(6ClBiPy)(CO)$_3$Cl]** complexation eluting around 5.2 min. The HPLC elution of [^{18}F]**6FBiPy** from this two-reactor experiment slightly differs from the elution of **6ClBiPy** from the non-radioactive single-reactor complexation experiment; however, as the gradient was held at 100 % aqueous phase for the first 2 min to ensure the retentions of [^{18}F]**6FBiPy** and [^{18}F]fluoride did not overlap. The peak identities were again verified via retention time comparisons with the non-radioactive **6FBiPy** and [**Re(6FBiPy)(CO)$_3$Cl**] standards using the UV channel. The observed RCYs can be rationalized through consideration of Figure 7, which depicts the rate constants for the forward and reverse reactions concerning: i) complexation (K_c) of **6ClBiPy** with **Re(CO)$_5$Cl** to form **[Re(6ClBiPy)(CO)$_3$Cl]** and reverse thermal dissociation (K_{-d}) of **[Re(6ClBiPy)(CO)$_3$Cl]** liberating **6ClBiPy**, ii) fluorination (K_f) of **[Re(6ClBiPy)(CO)$_3$Cl]** forming [^{18}F]**[Re(6FBiPy)(CO)$_3$Cl]** and reverse defluorination (K_{-df}) with formerly displaced chloride ions forming **[Re(6ClBiPy)(CO)$_3$Cl]**, and iii) thermal dissociation (K_d) of [^{18}F]**[Re(6FBiPy)(CO)$_3$Cl]** to liberate [^{18}F]**6FBiPy** and reverse complexation (K_{-c}) with excess **Re(CO)$_5$Cl** to reform the [^{18}F]**[Re(6FBiPy)(CO)$_3$Cl]** labelled complex. The fluorination of **6ClBiPy** is too slow afford an appreciable rate constant, as evidenced by the 96 h synthesis time of the non-radioactive standard and our former experiments demonstrating no discernible yield of [^{18}F]**6FBiPy** from the ligand precursor.[14] Reactions between [^{18}F]TBAF and **Re(CO)$_5$Cl** across the trialed temperatures likewise afforded no radioproducts. Thus, the incorporation of fluorine-18 is principally restricted to the radioactive species illustrated in Figure 7. For reactions at temperatures 50 and 70 °C, the K_c rate constant is clearly lower in value thus resulting in minimal **[Re(6ClBiPy)(CO)$_3$Cl]** required to form the radioproducts from subsequent fluorination. For temperatures of 90 °C onwards it is curious to note how differences in the MR1 temperature affected radiotracer production, given that the K_f and K_d rate constants should remain unperturbed given the stable 190 °C MR2 temperature. Evidently, the amount of [^{18}F]**[Re(6FBiPy)(CO)$_3$Cl]** and [^{18}F]**6FBiPy** formed was linked to the amount of **[Re(6ClBiPy)(CO)$_3$Cl]** produced in MR1. Between the 90–130 °C temperature range, a reasonable quantity of **[Re(6ClBiPy)(CO)$_3$Cl]** was radiofluorinated to form [^{18}F]**[Re(6FBiPy)(CO)$_3$Cl]** in solution, though not enough to warrant significant dissociation. Whereas between 150–190 °C, within the range previously confirmed to afford optimum complexation, a greater quantity of complex was fluorinated to afford [^{18}F]**[Re(6FBiPy)(CO)$_3$Cl** which in turn afforded a greater RCY of [^{18}F]**6FBiPy**. These results suggest that with a longer residence time in MR2 for the 90–130 °C temperature range, the RCY of [^{18}F]**6FBiPy** could have been improved, as both reactions are governed by the K_c and K_d rate constants. While rapid heat transfer in microfluidic laminar flow systems would be expected, it could be possible that the residual heat of the reaction bolus leaving MR1 affected reactions at MR2 by reducing the time required for uniform heating in the coil, thus accounting for the significant difference in RCYs at higher temperatures.

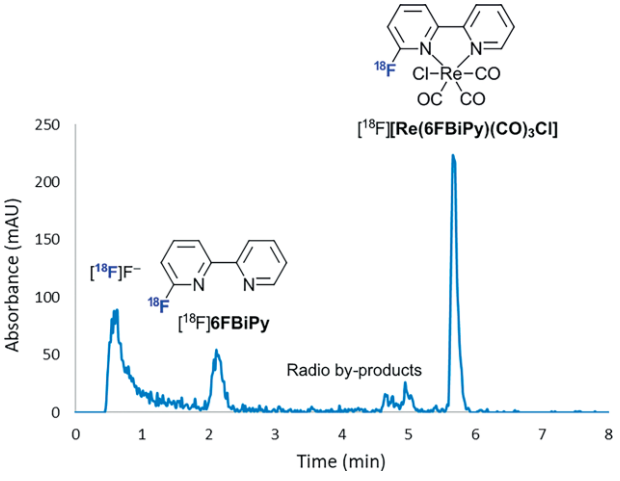

Figure 6. Radiochromatogram acquired from the complexation and radiofluorination of [**Re(6ClBiPy)(CO)$_3$Cl**], with MR1 set to 130 °C and MR2 set to 190 °C, depicting the retention of [^{18}F]**6FBiPy** at 2.15 min and [^{18}F][**Re(6FBiPy)(CO)$_3$Cl**] at 5.68 min. The gradient was held at 100 % water for the first 2 min to avoid coelution of [^{18}F]6FBiPy with [^{18}F]fluoride. A full description of the HPLC gradient profile is provided in Table 3 of Section 4 – Materials and Methods.

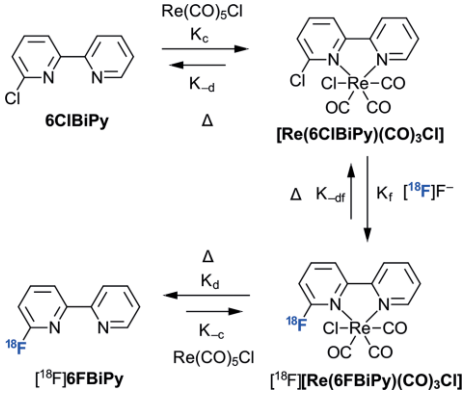

Figure 7. Rate constants for the forward and reverse reactions concerning complexation (K_c), reverse dissociation [K_{jd}], fluorination (K_f), reverse defluorination [K_{jdf}], dissociation (K_d) and reverse complexation [K_{jc}] leading to the formation of [^{18}F]**6FBiPy**.

Given the promising dual-reactor in-flow production of [^{18}F]**6FBiPy**, we were keen to translate the design methodology to the production of [^{18}F]**CABS13**, an AD PET diagnostic agent. The synthetic routes used to obtain the precursors for radiosynthesis and non-radioactive standards for retention time compar-

Full Paper
doi.org/10.1002/ejic.202000433

isons is illustrated in Figure 8. A solution of **$Re(CO)_5Cl$** was first refluxed in acetonitrile under anhydrous and deoxygenated conditions to afford the **$[Re(CO)_3(NCCH_3)_2Cl]$** intermediate, to which **2Cl8HQ** was added and further refluxed. The resulting **$[Re(2Cl8HQ)(CO)_3(NCCH_3)]$** complex was then found to precipitate from solution. Formation of the non-radioactive fluorinated standards required additional steps of synthesis. 2-chloro-8-hydroxyquinoline (**2Cl8HQ**) was first dissolved in dimethylformamide (DMF) and treated with benzyl chloride in the presence of potassium carbonate to afford the **2Cl8HQ-OBn** benzyl protected alcohol. Subsequent fluorination using potassium fluoride and an 18-crown-6 PTC in DMSO afforded **CABS-13-OBn**, which was then reduced over hydrogen gas in the presence of palladium and palladium hydroxide on carbon catalysts in acetonitrile solution to afford the **CABS13** standard. The **CABS13** ligand was then complexed with the **$[Re(CO)_3(NCCH_3)_2Cl]$** intermediate, again formed from refluxing **$Re(CO)_5Cl$** in acetonitrile, to afford the desired **$[Re(CABS13)(CO)_3(NCCH_3)]$** fluorinated standard.

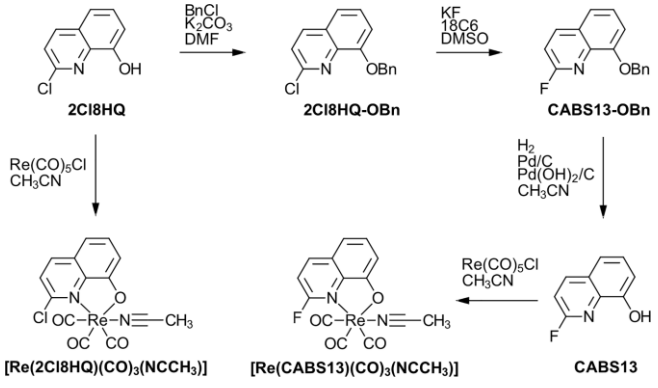

Figure 8. Synthetic route used to obtain the **2Cl8HQ** and **$[Re(2Cl8HQ)(CO)_3(NCCH_3)]$** precursors, as well as the **CABS13** and **$[Re(CABS13)(CO)_3(NCCH_3)]$** non-radioactive standards.

As radiosyntheses of [^{18}F]**CABS13** can be particularly low yielding, the microfluidic set-up was further modified to incorporate three microreactors in series, as shown in Figure 9. The temperatures were modified to control the rates of complexation, fluorination and dissociation at MR1, MR2 and MR3, respectively. An additional radioactivity detector was placed near the site of MR3 to monitor entry and departure of the radioactive solution into the final product vial for radioHPLC analysis. In this particular set-up P1 delivered a solution of **2Cl8HQ** (0.88 mg mL^{-1}, 4.88 μmol mL^{-1}) in DMSO, whereas P2 continued to supply **$Re(CO)_5Cl$** (2.12 mg mL^{-1}, 5.86 μmol mL^{-1}) dissolved in acetonitrile. P3 and P4 reprised the former roles of azeotropically drying and supplying the [^{18}F]TEAF solution in DMSO. Boluses (20 μL) of **2Cl8HQ** and **$Re(CO)_5Cl$** were pumped through to MR1 in a 1:1 volumetric ratio, ensuring an excess 1.20 equiv. of **$Re(CO)_5Cl$**, and each at a flow rate of 5 μL min^{-1}. Thus, the summative flow rate of 10 μL min^{-1} in the 15.6 μL void volume of MR1 resulted in a residence time of 94 s. P3 supplied the [^{18}F]TEAF (61 ± 14 MBq) solution at a rate of 10 μL min^{-1}, thus resulting in a cumulative flow rate of 20 μL min^{-1} in both MR2 and MR3. Given that the internal volumes (31.2 μL) were the same for both MR1 and MR2, the residence time of the reaction boluses was also 94 s in all microreactors. Figure 10 depicts the rate constants for the forward and reverse reactions intended to be controlled at each microreactor; i) complexation (K_c) of **2Cl8HQ** with **$Re(CO)_5Cl$** to form **$[Re(2Cl8HQ)(CO)_3(NCCH_3)]$** at MR1 and reverse thermal dissociation (K_{-d}) of **$[Re(2Cl8HQ)(CO)_3(NCCH_3)]$** liberating **2Cl8HQ**, ii) fluorination (K_f) of **$[Re(2Cl8HQ)(CO)_3(NCCH_3)]$** forming [^{18}F]**$[Re(CABS13)(CO)_3(NCCH_3)]$** at MR2 and reverse defluorination (K_{df}) with formerly displaced chloride ions forming **$[Re(2Cl8HQ)(CO)_3(NCCH_3)]$**, and iii) thermal dissociation (K_d) of [^{18}F]**$[Re(CABS13)(CO)_3(NCCH_3)]$** to liberate [^{18}F]**CABS13** at MR3 and reverse complexation (K_{-c}) with excess **$Re(CO)_5Cl$** to reform the [^{18}F]**$[Re(CABS13)(CO)_3(NCCH_3)]$** labelled complex. Table 2 lists

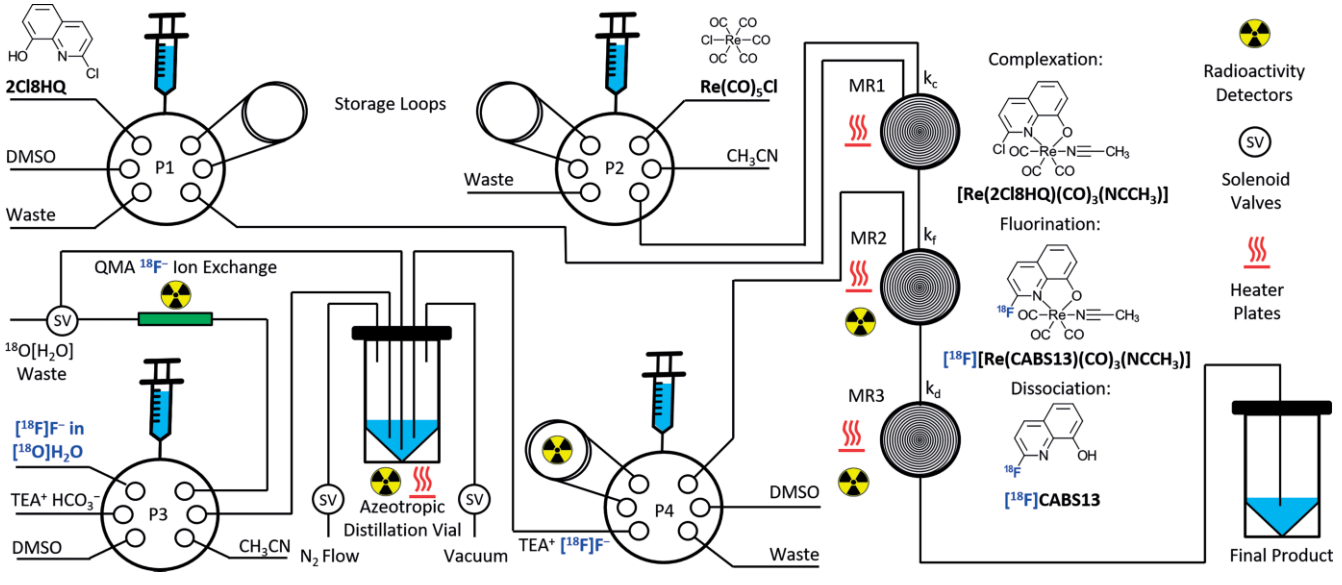

Figure 9. Triple reactor microfluidic set-up for the complexation of **6ClBiPy** with $Re(CO)_5Cl$ in MR1 to afford **$[Re(6ClBiPy)(CO)_3Cl]$**, followed by radiofluorination to afford [^{18}F]**$[Re(6FBiPy)(CO)_3Cl]$** in MR2 and dissociation in MR3 to afford [^{18}F]**6FBiPy**.

Full Paper
doi.org/10.1002/ejic.202000433

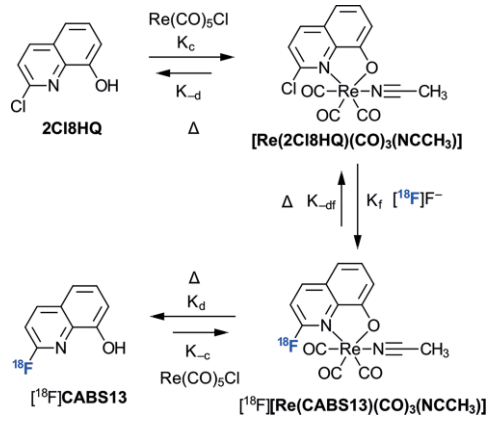

Figure 10. Rate constants for the forward and reverse reactions concerning complexation (K_c), reverse dissociation (K_{-d}), fluorination (K_f), reverse defluorination (K_{-df}), dissociation (K_d) and reverse complexation (K_{-c}) leading to the formation of [^{18}F]**CABS13**.

the RCYs for [^{18}F]**CABS13** and [^{18}F]**[Re(CABS13)(CO)$_3$(NCCH$_3$)Cl]** determined from radioHPLC analyses of each solution acquired from modulation of the three microreactor temperatures. The incorporation of both DMSO and acetonitrile solvents would have resulted in continuous exchange at the rhenium(I) coordination sphere, given the lability of both ligands. However, as acetonitrile was used in the HPLC eluent mobile phase, any coordinated DMSO ligand was likely displaced for acetonitrile during radioHPLC analysis, thus leading to the observed retention time comparison around 7.5 min with the non-radioactive standard. The amount of both radioproducts formed were relatively the same, independent of the temperatures applied to the microreactors, with the RCY of [^{18}F]**CABS13** ranging between 1.2–2.7 % and the RCY of [^{18}F]**[Re(CABS13)(CO)$_3$(NCCH$_3$)Cl]** ranging between 1.0–1.9 %. The highest yield of 2.7 % [^{18}F]**CABS13** was acquired through temperatures of 130 °C applied to MR1 and 190 °C applied to both MR2 and MR3. Whereas the highest yield of 1.9 % [^{18}F]**[Re(CABS13)(CO)$_3$(NCCH$_3$)Cl]** was obtained through applying temperatures of 170 °C to MR1 and MR2, followed by 190 °C at MR3. These comparatively low yields could be rationalized through a particularly low K_c rate constant which constrained the amount of **[Re(2Cl8HQ)(CO)$_3$(NCCH$_3$)]** present to form the desired radiotracers through the subsequent K_f and K_d channels. However, higher MR1 temperatures in our former complexation studies appeared to favour thermal decomplexation represented by the K_{-d} pathway, and hence further modulation of the MR1 temperature conditions were discontinued. These former complexation studies were trialed solely in DMSO media, and the laminar composition of acetonitrile with DMSO could in part account for the lesser RCYs. Nonetheless, one final experiment using this microfluidic set-up was undertaken, whereby the temperature of MR3 was increased to 210 °C. The temperature represents the upper end of our instrumental capabilities which we do not routinely apply for sustainability purposes, hence why all other reactions did not exceed 190 °C. Applying temperatures of 130, 190 and 210 °C at MR1, MR2 and MR3, respectively, still only resulted in middle range RCYs of 1.7 % [^{18}F]**CABS13** and 1.5 % [^{18}F]**[Re(CABS13)(CO)$_3$(NCCH$_3$)Cl]**.

Suspecting the lower RCYs of [^{18}F]**CABS13** and [^{18}F]**[Re(CABS13)(CO)$_3$(NCCH$_3$)]** to be principally linked to the quality of the solvents employed, we repeated the single reactor microfluidic experiment employing the **[Re(2Cl8HQ)(CO)$_3$(NCCH$_3$)]** precursor (0.80 μmol) dissolved in DMSO. The precursor was treated with [^{18}F]TEAF (29 ± 10 MBq) over a 7.80 min residence time in a microreactor heated to 190 °C. Such conditions formerly yielded 5 % [^{18}F]**CABS13** and 18 % [^{18}F]**[Re(CABS13)(CO)$_3$(NCCH$_3$)]**.[14] However, when repeating this experiment we found the yields to be approximately half as those expected, with [^{18}F]**CABS13** being produced in only 2.3 % RCY and [^{18}F]**[Re(CABS13)(CO)$_3$(NCCH$_3$)]** being produced in only 9.8 % RCY, as shown by the radiochromatogram in Figure 11. The only significant change between this experimental set-up and the previous was the anhydrous DMSO solvent employed, which was replaced as a cost-saving initiative within our department. Formerly we had used ≥ 99.9 % anhydrous DMSO purchased from Sigma-Aldrich (product ID: 276855), whereas for the experiments reported in this work we used ≥ 99.7 % DMSO purchased from Merck Millipore (product ID: 109678). This was before Merck recently acquired Sigma-Aldrich for $17 billion USD.[18] Evidently, the 0.2 % of water makes a considerable difference due to the low concentrations and sensitivity of radiochemical reactions employing fluorine-18. Such a requirement for anhydrous radiofluorination conditions has been observed in the production of many radiopharmaceutical agents.[19] Despite the routine azeotropic drying of the fluorination media, as all of the reagents were dissolved in DMSO with a slightly higher water content it would

Table 2. RCYs of [^{18}F]**CABS13** and [^{18}F]**[Re(CABS13)(CO)$_3$(NCCH$_3$)]** obtained from in-flow radiosyntheses applying MR1 (non-radioactive complexation), MR2 (radiofluorination) and MR3 (thermal dissociation) microreactors in-series at the specified temperatures.

MR1 Temperature [°C]	MR2 Temperature [°C]	MR3 Temperature [°C]	[^{18}F]CABS13 (% RCY)	[^{18}F][Re(CABS13)(CO)$_3$(NCCH$_3$)] (% RCY)
130	150	190	1.2	1.0
130	170	190	1.5	1.2
130	190	190	2.7	1.8
150	190	190	2.1	1.6
150	150	190	2.0	1.7
150	170	190	2.1	1.7
170	170	190	2.1	1.9
170	190	190	1.9	1.7
190	190	190	1.8	1.8
130	190	210	1.7	1.5

Full Paper
doi.org/10.1002/ejic.202000433

appear that the RCYs of [^{18}F]**CABS13**, [^{18}F]**6FBiPy** and their respective rhenium(I) complexes were all comparatively lower than our former experiments.[14] This is despite the implementation of multiple reactors which should otherwise have improved the reaction RCYs. Nonetheless, our former experiments have fortunately shown that radiofluroinations of rhenium(I) complexes can tolerate slightly hydrous conditions to afford radioproducts and, as such, the data presented here still provides a useful analysis of which temperature conditions are best utilized in multireactor in-flow complexation reactions.

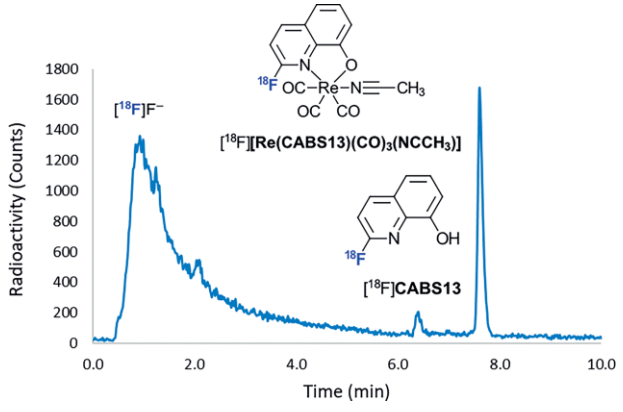

Figure 11. Radiochromatogram showing the formation of [^{18}F]**CABS13** in 2.3 % RCY (6.32 min) and [^{18}F]**[Re(CABS13)(CO)$_3$(NCCH$_3$)]** in 9.8 % RCY (7.58 min). The gradient was held at 100 % water for the first 3 min to avoid coelution of [^{18}F]CABS13 with [^{18}F]fluoride. A full description of the HPLC gradient profile is provided in Table 3 of Section 4 – Materials and Methods.

Further considerations for increasing the yield of [^{18}F]CABS13, which were not implemented herein, could involve the use of an acid primed solid supported reagent to assist in dissociation of the metal centre or the use of light-induced photodissociation in flow.[20] Photodissociation methods, specifically, have been widely applied in the decomplexation of similar group VII manganese(I) tricarbonyl complexes, typically in application to carbon monoxide therapies and antibacterial activity.[21] Such methods could potentially improve the efficiency of rhenium(I) decomplexation strategies and widen the scope of fluorine-18 labelled radiopharmaceuticals for which the complexation-dissociation reaction could be applied to.

3. Conclusions

Herein, the radiosynthesis of the [^{18}F]**CABS13** AD PET neuroimaging agent has been simplified to a single microfluidic set-up incorporating three microreactors dedicated to the rhenium(I) complexation, radiofluorination and dissociation of the ligand. Despite the compact set-up, the RCYs of [^{18}F]**CABS13** and the [^{18}F]**[Re(CABS13)(CO)3(NCCH$_3$)]** complex were comparatively lower than former single microreactor set-ups. Repeat analyses of the single-reactor conditions were found to also afford lower RCYs which were linked to the different grades of anhydrous DMSO solvents used in the experiments. Here we highlight the significant impact of a 0.2 % difference in water content on radiofluorination reactions. This trend was likewise noted in our dual microreactor experiments designed to improve [^{18}F]**6FBiPy** and [^{18}F]**[Re(6FBiPy)(CO)$_3$Cl]** syntheses, which also afforded lower RCYs when compared to our previously reported single-reactor experiments with the same reagents. However, it cannot be overlooked that the lower RCYs could also be the result of lesser complexation at the first microreactor and replicate experiments using ≤ 99.9 % anhydrous DMSO would be needed to verify this hypothesis. Nonetheless, we have demonstrated that in-flow rhenium(I) complexation reactions are indeed feasible under microfluidic conditions and that such products can be telescoped for subsequent radiolabelling with fluorine-18. These results mark significant progress towards the automated manufacturing of similar reagents, and we have demonstrated the optimum temperature conditions required to balance the competing complexation and dissociation pathways towards heightened RCYs.

4. Experimental Section

Materials and Methods: Instruments and Reagents: NMR analyses were performed using a Bruker Spectrospin 400 MHz UltraShield NMR spectrometer. Fourier transform infrared (FTIR) analyses were performed using a Bruker ALPHA-p IR spectrometer. UV/Vis analyses were performed using an Agilent technologies Cary 100 UV/Vis spectrometer. Low resolution mass spectrometry (LRMS) analyses were performed using a Waters micromass ZQ, equipped with an electrospray ionisation (ESI) source running in positive ionisation mode with the following parameters applied; voltages: 3 kV capillary voltage, 25 V cone voltage for organic molecules and 70 V cone voltage for rhenium complexes (required to dissociate Re–Cl bonds), 5 V extractor voltage and 0.2 V radiofrequency (RF) lens voltage; Temperatures: 45 °C source temperature and 300 °C desolvation temperature; and gas flows: 350 L h^{-1} desolvation nitrogen gas flow and 90 L h^{-1} cone nitrogen gas flow. Samples for high resolution mass spectrometry (HRMS) were sent to the Mass Spectrometry User Resource and Research Facility at the University of Wollongong and samples for elemental analysis (EA) were sent to the Campbell Microanalytical Laboratory at the University of Otago. All synthetic reagents were purchased from Sigma-Aldrich except for trifluoroacetic acid (TFA) and 18-crown-6 ether which were purchased from Alfa Aesar, and 2-chloro-2,2′-bipyrdine and 2-chloro-8-hydroxyquinoline which were purchased from Bepharm. Finally, all solvents were purchased from Merck Millipore, including DMSO (product ID: 109678), and all water solutions used for syntheses and analyses were first purified using a Merck Millipore Milli-Q integral water purification system.

Non-Radioactive Syntheses of Standards and Precursors

Tricarbonylchloro(6-chloro-2,2′-bipyridine)rhenium(I) Chloride ([Re(6ClBiPy)(CO)$_3$Cl]): A mass of **6ClBiPy** (277.5 mg, 1.456 mmol, 1.1 equiv.) was dissolved in a volume of anhydrous toluene (5 mL). A mass of pentacarbonylrhenium(I) chloride (478.7 mg, 1.3234 mmol, 1.0 equiv.) was then added and the solution was stirred at reflux under an inert nitrogen environment (5 h). The solution was then cooled to –20 °C to afford a precipitate. The precipitate was isolated via vacuum filtration and was washed with cold diethyl ether. The crude material was then purified over a neutral Brockman grade II alumina stationary phase using a DCM mobile phase. The combined fractions were evaporated under reduced pressure to afford a pure yellow powder (564.2 mg, 86 % yield). ^{1}H NMR (400 *MHz*, [D$_6$]DMSO, δ/*ppm*): δ 9.06 (d, J^d = 4.76 *Hz*, 1H), δ = –8.76 (d, J^d = 8.12 *Hz*, 2H),

δ 8.35 (*app.* td, J^d = 1.96, J^t = 8.04 *Hz*, 2H), δ 8.08 (dd, J^d = 0.68, 8.04 *Hz*, 1H), δ 7.78 (*app.* td, J^d = 1.80, J^t = 4.56 *Hz*, 1H). $^{13}C\{^1H\}$ NMR (100 *MHz*, [D_6]DMSO, δ/*ppm*): δ = 197.5$_{C\equiv O}$, δ = 197.3$_{C\equiv O}$, δ = 189.5$_{C\equiv O}$, δ = 157.2, δ = 155.6, δ = 153.2, δ = 152.8, δ = 142.7, δ = 140.3, δ = 128.0, δ = 127.7, δ 125.3, δ = 123.1. FTIR (ATR *corr.* $\tilde{\nu}$ = / cm^{-1}): $\tilde{\nu}$ 3075 (w, C–H sp^2 *str.*), $\tilde{\nu}$ 2018 (s, A′(1) C≡O *str.*), $\tilde{\nu}$ 1882 (s, A′(2) & A″ C≡O *str.*). UV/Vis (λ/*nm*, ε/*L mol*$^{-1}$ cm^{-1}): λ 380 ($d\pi\rightarrow\pi^*$, ε 3375.36), λ 301 ($\pi\rightarrow\pi^*$, ε 14990.57), λ 326 ($\pi\rightarrow\pi^*$, ε 10920.28), λ 233 ($\pi\rightarrow\pi^*$, ε 19259.41). LRMS (ESI^+): $[M - Cl]^+$ *m/z* cald: 460.97, *m/z* obvs. 460.95. HRMS (ESI^+): $[M - Cl]^+$ *m/z* cald: 460.9703, *m/z* obvs. 460.9694 (Δ –2.0 *ppm*). EA (%): *calcd.* C 31.46, H 1.42, N 5.64. *found* C 31.59, H 1.17, N 5.70.

6-Fluoro-2,2′-bipyridine (6FBiPy): A mass of **6ClBiPy** (318.7 mg, 1.672 mmol, 1.0 equiv.) was dissolved in a volume of anhydrous DMSO (10 mL). Masses of potassium fluoride (1.712 g, 29.466 mmol, 17.6 equiv.) and 18-crown-6 ether (1.567 g, 5.928 mmol, 3.5 equiv.) were azeotropically dried via dropwise addition of anhydrous acetonitrile at 90 °C under an inert nitrogen gas flow. The ligand solution was then added to the dried reagents, heated to 90 °C and stirred under an inert nitrogen environment (96 h). The solution was then cooled and filtered through a polytetrafluoroethylene (PTFE) membrane (0.2 μm). The filtrate was then purified via reverse phase chromatography employing a C_{18} stationary phase and an acetonitrile/TFA (0.1 % in water) mobile phase. Lyophilization of the combined fractions afforded a pink salt which was dissolved in a minimum of water (20 mL), neutralized with sodium bicarbonate and extracted into DCM. The combined organic fractions were then dried with sodium sulfate and evaporated under reduced pressure to afford a white powder (39.2 mg, 13 % yield). ^1H NMR (400 *MHz*, $CDCl_3$, δ/*ppm*): δ 8.74 (d, J^d = 4.20 *Hz*, 1H), δ 8.50 (d, J^d = 6.48 *Hz*, 1H), δ 8.45 (d, J^d = 8.04 *Hz*, 1H), δ 7.96 (q, J^q = 15.84, 8.00 *Hz*, 2H), δ 7.45 (d, J^t = 6.52 *Hz*, 1H), δ 7.00 (dd, J^d = 8.08, 2.80 *Hz*, 1H). $^{13}C\{^1H\}$ NMR (100 *MHz*, $CDCl_3$, δ/*ppm*): δ = 163.3 (d, J^d = 237 *Hz*), δ = 155.1 (d, J^d = 13 *Hz*), δ = 154.7, δ = 149.4, δ = 142.0 (d, J^d = 7 *Hz*), δ = 137.2, δ = 124.3, δ = 121.4, δ = 118.3 (d, J^d = 4 *Hz*), δ = 109.6 (d, J^d = 37 *Hz*). $^{19}F\{^1H\}$ NMR (376 *MHz*, $CDCl_3$, δ/*ppm*): δ = –66.77. LRMS (ESI^+): $[M + H]^+$ *m/z* cald: 175.07, *m/z* obvs. 175.14.

Tricarbonylchloro(6-fluoro-2,2′-bipyridine)rhenium(I) Chloride ([Re(6ClBiPy)(CO)$_3$Cl]): A mass of **6FBiPy** (65.3 mg, 0.363 mmol, 1.1 equiv.) was dissolved in a volume of anhydrous toluene (8 mL). A mass of pentacarbonylrhenium(I) chloride (120.0 mg, 0.323 mmol, 1.0 equiv.) was then added and the solution was stirred at reflux under an inert nitrogen environment (3 h). The solution was then cooled to –20 °C to afford a precipitate. The precipitate was isolated via vacuum filtration and was washed with cold diethyl ether. The crude material was then purified over a neutral Brockman grade II alumina stationary phase using a DCM mobile phase. The combined fractions were evaporated under reduced pressure to afford a pure yellow powder (104.1 mg, 65 % yield). ^1H NMR (400 *MHz*, [D_6]DMSO, δ/*ppm*): δ 9.06 (*app.* tq, J^t = 5.48 *Hz*, J^q = 0.80 *Hz*, 1H), δ 8.80 (d, J^d = 8.16 *Hz*, 1H), δ 8.70 (d, J^d = 7.92 *Hz*, 1H), δ 8.52 (q, J^q = 8.04 *Hz*, 1H), δ 8.36 (td, J^t = 8.08 *Hz*, J^d = 1.52 *Hz*, 1H), δ 7.80 (m, 2H). $^{13}C\{^1H\}$ NMR (100 *MHz*, [D_6]DMSO, δ/*ppm*): δ = 197.2$_{C\equiv O}$, δ = 196.6$_{C\equiv O}$ (d, J^d = 16.59 *Hz*), δ = 188.9$_{C\equiv O}$, δ = 164.0, δ = 161.5, δ = 154.4 (d, J^d = 15.92 *Hz*), δ = 153.1, δ = 145.9 (d, J^d = 10.15 *Hz*), δ = 140.4, δ = 128.2, δ 125.1, δ = 121.4 (d, J^d = 2.94 *Hz*), δ = 112.7 (d, J^d = 30.19 *Hz*). $^{19}F\{^1H\}$ NMR (376 *MHz*, [D_6]DMSO, δ/*ppm*): δ –51.75. FTIR (ATR *corr.* $\tilde{\nu}$ = /cm^{-1}): $\tilde{\nu}$ 3040 (w, C–H sp^2 *str.*), $\tilde{\nu}$ 2016 (s, A′(1) C≡O *str.*), $\tilde{\nu}$ 1880 (s, A′(2) & A″ C≡O *str.*). UV/Vis (λ/*nm*, ε/*L mol*$^{-1}$ cm^{-1}): λ 369 ($d\pi\rightarrow\pi^*$, ε 2768.36), λ 296 ($\pi\rightarrow\pi^*$, ε 12485.88), λ 235 ($\pi\rightarrow\pi^*$, ε 15367.33). LRMS (ESI^+): $[M - Cl]^+$ *m/z* cald: 445.00, *m/z* obvs. 445.10. EA (%): *calcd.* C 32.54, H 1.47, N 5.84. *found* C 32.59, H 1.16, N 5.88.

Acetonitriletricarbonyl(2-chloro-8-quinolinolate)rhenium(I) ([Re(2Cl8HQ)(CO)$_3$Cl]): A mass of pentacarbonylrhenium(I) chloride (116.1 mg, 0.321 mmol, 1.0 equiv.) was added to a volume of anhydrous acetonitrile (10 mL) and refluxed in an inert nitrogen environment (4 h) to afford the diacetonitriletricarbonlylrhenium(I) chloride intermediate. A mass of **2Cl8HQ** (63.4 mg, 0.353 mmol, 1.1 equiv.) was dissolved in a volume of anhydrous acetonitrile (2 mL) and deprotonated via the addition of sodium hydride (48.0 mg, 2.000 mmol, 6.2 equiv.) over a 0 °C ice bath. The resulting green solution was then filtered through a PTFE membrane (0.2 μm) and added to the intermediate solution and left to stir at room temperature under an inert nitrogen environment (12 h). A volume of aqueous trifluoromethanesulfonic acid (0.1 mol L^{-1}, 10 mL) was then added. The solution was evaporated under reduced pressure to afford a yellow solid in aqueous suspension. The precipitate was isolated via vacuum filtration and purified over a neutral Brockmann grade II alumina stationary phase using an acetonitrile mobile phase. The combined fractions were then evaporated under reduced pressure to afford a yellow powder (49.8 mg, 32 % yield). ^1H NMR (400 *MHz*, CD_3CN, δ/*ppm*): δ 8.32 (d, J^d = 8.68 *Hz*, 1H), δ 7.58 (d, J^d = 8.68 *Hz*, 1H), δ 7.43 (t, J^t = 7.96 *Hz*, 1H), δ 7.01 (dd, J^d = 7.96, 0.96 *Hz*, 1H), δ = 6.92 (dd, J^d = 7.96, 1.04 *Hz*, 1H), δ 1.96 (s, 3H). $^{13}C\{^1H\}$ NMR (100 *MHz*, CD_3CN, δ/*ppm*): δ = 196.6$_{C\equiv O}$, δ 195.3$_{C\equiv O}$, δ 195.3$_{C\equiv O}$, δ = 170.2, δ = 152.3, δ = 144.3, δ = 142.6, δ = 131.2, δ = 130.1, δ = 123.8, δ = 120.8, δ 117.7, δ = 112.4, δ = 30.3. FTIR (ATR *corr.* $\tilde{\nu}$ = /cm^{-1}): $\tilde{\nu}$ 2925.41 (w, C–H sp^2 *str.*), $\tilde{\nu}$ 2303.92 (w, N≡C *str.*), $\tilde{\nu}$ 2016.96 (s, A′(1) C≡O *str.*), $\tilde{\nu}$ 1871.84 (s, A′(2) & A″ C≡O *str.*). UV/Vis (λ/*nm*, ε/*L mol*$^{-1}$ cm^{-1}): λ 437 ($d\pi\rightarrow\pi^*$, ε 235.06), λ 281 ($\pi\rightarrow\pi^*$, ε 2340.84), λ 237 ($\pi\rightarrow\pi^*$, ε 3104.80). EA (%): calcd. C 34.32, H 1.65, N 5.72. *found* C 34.89, H 1.54, N 5.60.

2-Chloro-8-benzoxyquinoline (2Cl8HQ-OBn): A mass of **2Cl8HQ** (2.40 g, 13.4 mmol, 1.0 equiv.) was dissolved in a volume of anhydrous DMF (2.5 mL) alongside a mass of potassium carbonate (3.69 g, 26.7 mmol, 2.0 equiv.). A volume of benzyl chloride (3.1 mL, 27.4 mmol, 2.0 equiv.) was added dropwise to the solution. The reaction was stirred at 60 °C in an inert nitrogen environment (3 h). The solution was then cooled and extracted with DCM (20 × 10 mL). The combined organic extracts were washed with brine (3 × 20 mL). The solution was then dried with sodium sulfate and evaporated under reduced pressure. Recrystallisation from hot ethanolic solution afforded a pure pink product (3.0 g, 85 % yield). ^1H NMR (400 *MHz*, $CDCl_3$, δ/*ppm*): δ 8.06 (d, J^d = 8.60 Hz, 1H), δ 7.50 (d, J^d = 7.36 Hz, 1H), δ 7.40 (d, J^d = 8.56 Hz, 1H), δ 7.36 (m, 1H), δ 7.30 (d, J^d = 7.06 Hz, 1H), δ 7.06 (dd, J^d = 6.08, 3.00 Hz, 1H). $^{13}C\{^1H\}$ NMR (100 *MHz*, $CDCl_3$, δ/*ppm*): δ = 153.7, δ = 150.0, δ = 140.0, δ = 138.7, δ = 137.0, δ = 128.7, δ = 128.3, δ = 127.9, δ = 127.2, δ = 127.1, δ = 127.1, δ = 123.1, δ 119.7, δ = 111.8, δ 71.0.

2-Fluoro-8-benzoxyquinoline (CABS13-OBn): A mass of **2Cl8HQ-OBn** (1.48 g, 5.5 mmol, 1.0 equiv.) was dissolved in a volume of anhydrous DMSO (10 mL). Masses of potassium fluoride (3.84 g, 66.1 mmol, 12.0 equiv.) and 18-crown-6 ether (5.84 g, 22.1 mmol, 4.0 equiv.) were azeotropically dried via dropwise addition of anhydrous acetonitrile at 90 °C under an inert nitrogen gas flow. The ligand solution was then added to the dried reagents, heated to 160 °C and stirred under an inert nitrogen environment (12 days). The solution was then cooled and filtered through a polytetrafluoroethylene (PTFE) membrane (0.2 μm). The filtrate was purified via reverse phase chromatography employing a C_{18} stationary phase and an acetonitrile/TFA (0.1 % in water) mobile phase. Lyophilization of the combined fractions afforded a pink salt which was dissolved in a minimum of water (60 mL), neutralized with sodium bicarbonate and extracted into DCM. The combined organic fractions were then dried with sodium sulfate and evaporated under

reduced pressure to afford a white powder (357 mg, 26 % yield). MP: 107 °C, 26 % yield. ^{1}H NMR (400 *MHz*, $CDCl_3$, δ/*ppm*): δ 8.22 (d, J^d = 8.40 Hz, 1H), δ 7.51 (d, J^d = 7.40 Hz, 1H), δ 8.35 (m, 5H), δ 7.10 (m, 2H), δ 5.42 (s, 1H). ^{13}C{^{1}H} NMR (100 *MHz*, $CDCl_3$, δ/*ppm*): δ = 162.0, δ = 159.5, δ = 153.6 (J^d = 2 *Hz*), δ = 142.1 (J^d = 9 *Hz*), δ = 137.7 (J^d = 15 *Hz*), δ = 137.0, δ = 128.8, δ = 128.2 (J^d = 2 *Hz*), δ = 128.0, δ = 127.2, δ = 126.3 (J^d = 9 *Hz*), δ 119.7, δ = 111.8, δ = 110.9, δ = 110.4. ^{19}F{^{1}H} NMR (376 *MHz*, [D_6]DMSO, δ/*ppm*): δ = –61.07.

2-Fluoro-8-hydroxyquinoline (CABS13): A mass of **2F8HQ-OBn** (218 mg, 0.859 mmol, 1.0 equiv.) was dissolved in a volume of anhydrous acetonitrile (6 mL). Masses of 10wt.-% palladium on activated carbon (123 mg) and 20wt.-% palladium hydroxide on activated carbon (125 mg) were added to the reaction in an inert nitrogen environment. The reaction flask was purged with hydrogen gas and left to stir (1 h). The solution was filtered through diatomaceous earth to afford a yellow filtrate. The filtrate was evaporated under reduced pressure and recrystallised from hot ethanolic solution to afford a white powder (106 mg), 75 % yield). MP: 62 °C; ^{1}H NMR (400 *MHz*, [D_6]DMSO, δ/*ppm*): δ 9.89 (br. s, 1H), δ 8.51 (t, J^t = 8.60 *Hz*), δ 7.45 (m, 2H), δ 7.32 (dd, J^d = 8.80, 2.76 *Hz*, 1H), δ 7.14 (dd, J^d = 7.20, 1.64 *Hz*, 1H). ^{13}C{^{1}H} NMR (100 *MHz*, [D_6]DMSO, δ/*ppm*): δ = 159.6 (d, J^d = 238 *Hz*), δ = 152.5, δ = 143.0 (d, J^d = 10 *Hz*), δ = 135.4 (d, J^d = 15 *Hz*), δ = 127.9, δ = 126.9 (d, J^d = 2 *Hz*), δ 117.9, δ = 113.5, δ = 110.2 (d, J^d = 42 *Hz*). ^{19}F{^{1}H} NMR (376 *MHz*, [D_6]DMSO, δ/*ppm*): δ = –63.53. FTIR (ATR *corr.* $\tilde{\nu}$ = /cm^{-1}): $\tilde{\nu}$ 2473 (br. m, O-H *str.*).

Acetonitriletricarbonyl(2-fluoro-8-quinolinolate)rhenium(I) ([Re(2F8HQ)(CO)$_3$Cl]): A mass of pentacarbonylrhenium(I) chloride (79.6 mg, 0.220 mmol, 1.0 equiv.) was added to a volume of anhydrous acetonitrile (10 mL) and refluxed in an inert nitrogen environment (4 h) to afford the diacetonitriletricarbonylrhenium(I) chloride intermediate. A mass of **2Cl8HQ** (63.4 mg, 0.353 mmol, 1.1 equiv.) was dissolved in a volume of anhydrous acetonitrile (2 mL) and deprotonated via the addition of sodium hydride (7.2 mg, 0.3000 mmol, 1.4 equiv.) over a 0 °C ice bath. The resulting green solution was then filtered through a PTFE membrane (0.2 μm) and added to the intermediate solution and left to stir at room temperature under an inert nitrogen environment (12 h). A volume of aqueous trifluoromethanesulfonic acid (0.1 mol L^{-1}, 10 mL) was then added. The solution was evaporated under reduced pressure to afford a yellow solid in aqueous suspension. The precipitate was isolated via vacuum filtration and purified over a neutral Brockmann grade II alumina stationary phase using an acetonitrile mobile phase. The combined fractions were then evaporated under reduced pressure to afford a yellow powder (49.8 mg, 14 % yield). ^{1}H NMR (400 *MHz*, CD_3CN, δ/*ppm*): δ 8.51 (dd, J^d = 8.92, 7.04 *Hz*, 1H), δ 7.43 (t, J^t = 7.96 *Hz*, 1H), δ 7.33 (dd, J^d = 8.92, 1.24 *Hz*, 1H), δ 7.06 (d, J^d = 8.00 *Hz*, 1H), δ = 6.94 (d, J^d = 7.92 *Hz*, 1H). ^{13}C{^{1}H} NMR (100 *MHz*, CD_3CN, δ/*ppm*): δ 195.9$_{C\equiv O}$, δ = 194.9$_{C\equiv O}$, δ = 194.2$_{C\equiv O}$, δ = 168.0 (d, J^d = 2 *Hz*), δ = 161.5 (d, J^d = 256 *Hz*), δ = 145.0 (d, J^d = 2 *Hz*), δ = 139.7, δ = 129.6 (d, J^d = 2 *Hz*), δ = –128.6, δ = 116.5, δ = 111.5, δ = 109.8 (d, J^d = 33 *Hz*). ^{19}F{^{1}H} NMR (376 *MHz*, CD_3CN, δ/*ppm*): δ = –56.94. FTIR (ATR *corr.* $\tilde{\nu}$ = /cm^{-1}): $\tilde{\nu}$ 2925 (w, C–H sp^2 *str.*), $\tilde{\nu}$ 2853 (w, C–H sp^2 *str.*), $\tilde{\nu}$ 2322 (w, N≡C *str.*), $\tilde{\nu}$ 2020 (s, A′(1) C≡O *str.*), $\tilde{\nu}$ 1875 (s, A′(2) & A″ C≡O *str.*).

Protocol for Fluorine-18 Radiolabeling and Analysis: Aqueous [^{18}F]fluoride was produced on an IBA Cyclone 18 Twin Cyclotron via the ^{18}O(p,n)^{18}F reaction. Microfluidic radiosyntheses were performed in Discovery Mode using a NanoTek LF Microfluidic Synthesis System (Advion) connected to a standard laptop using NanoTek software v1.4.0 GMP Lite. Microreactors were made of fused silica tubing coiled tightly into a brass ring and held by a thermoresistant polymer. RadioHPLC analyses were carried out using a Shimadzu system comprised of a CBM-20 controller, LC-20AD pump, SIL-20AHT autoinjector, SPD-M20A PDA detector and a Lablogic Posi-RAM gamma detector. Analyses were performed using gradient conditions over 15 minutes, whereupon the aqueous phase was held for the first 2 minutes ([^{18}F]**6FBiPy** and complex) or 3 minutes ([^{18}F]**CABS13** and complex) followed by linear transposition from 95:5 to 5:95 water/acetonitrile over the remaining 12 or 13 minutes at a 2 mL min^{-1} flow rate (Table 3). Both water and acetonitrile mobile phases contained 0.1 % v/v of TFA buffer. A Chromolith RP column (monolith system, Merck 50 × 4.6 mm), demonstrated to have < 8 % [^{18}F]fluoride retention in low pH ranges,[22] was employed as the stationary phase. RadioHPLC derived non-isolated RCYs were calculated via the integrated peak area ratio between the radioproduct and other radioactive species present, inclusive of any unreacted [^{18}F]fluoride, using Laura V4.1.70 SP2 HPLC data analysis software. Integrations were performed over the appropriate 30 s retention time windows of the radiochromatograms corresponding to each peak; 1:50–2:20 min for [^{18}F]**6FBiPy**, 5:30–6:00 min for [^{18}F]**[Re(6FBiPy)(CO)$_3$Cl]**, 6:15–6:45 min for [^{18}F]**CABS13** and 7:30–8:00 min for [^{18}F]**[Re(CABS13)(CO)$_3$-(NCCH$_3$)]**.

Table 3. HPLC gradient profiles for the elution of [^{18}F]**6FBiPy** and [^{18}F]**[Re(6FBiPy)(CO)$_3$Cl]**, as well as [^{18}F]**CABS13** and [^{18}F]**[Re(CABS13)(CO)$_3$(NCCH$_3$)]**. Both analyses were acquired over 15.2 min, using a 2 mL min^{-1} flow rate over an octadecylsilane RP monolithic stationary phase (Merck Chromolith column). Both acetonitrile and water mobile phase solvents additionally contained 0.1 % v/v of TFA buffer.

Radiotracers	Time (min)	Acetonitrile [%]	Water [%]
	2	0	100
[^{18}F]6FBiPy and	0.1	5	95
[^{18}F][Re(6FBiPy)(CO$_3$)Cl]	13	95	5
	0.1	95	5
	3	0	100
[^{18}F]CABS13 and	0.1	5	95
[^{18}F][Re(CABS13)(CO$_3$)(NCCH$_3$)]	12	95	5
	0.1	95	5

Acknowledgments

This research was funded by the Australian Institute of Nuclear Science and Engineering (AINSE) via the provision of a Post-graduate Research Award (PGRA). The National Deuteration Facility (NDF) is partly funded by the National Collaborative Research Infrastructure Strategy (NCRIS), an Australian Government initiative. The authors thank Dr. Calina Betlazar for reviewing the manuscript. The authors thank Michael Tran and Dr. Gary Perkins for cyclotron production and National Imaging Facility (NIF) for support.

Keywords: Alzheimer's disease · Fluorine · Rhenium · Microfluidics · Flow chemistry

[1] a) M. M. Mielke, P. Vemuri, W. A. Rocca, *Clin. Epidemiol.* **2014**, *6*, 37–48; b) D. A. Casey, D. Antimisiaris, J. O'Brien, *Pharm. Ther.* **2010**, *35*, 208–211.
[2] Alzheimer's & Dementia **2016**, *12*, 459–509.
[3] Alzheimer's & Dementia **2019**, *15*, 321–387.
[4] a) D. S. Eisenberg, M. R. Sawaya, *Nature* **2017**, *547*, 170–171; b) M. Goedert, M. G. Spillantini, R. A. Crowther, *Brain Pathol.* **1991**, *1*, 279–286; c) C. Cicognola, G. Brinkmalm, J. Wahlgren, E. Portelius, J. Gobom, N. C. Cullen,

O. Hansson, L. Parnetti, R. Constantinescu, K. Wildsmith, H.-H. Chen, T. G. Beach, T. Lashley, H. Zetterberg, K. Blennow, K. Höglund, *Acta Neuropathol.* **2019**, *137*, 279–296; d) A. Metaxas, S. J. Kempf, *Neural. Regen. Res.* **2016**, *11*, 1579–1581.

[5] a) I. Benilova, E. Karran, B. D. e. Strooper, *Nat. Neurosci.* **2012**, *15*, 349–357; b) J. J. Palop, L. Mucke, *Nat. Neurosci.* **2010**, *13*, 812–818; c) R. M. Koffie, M. Meyer-Luehmann, T. Hashimoto, K. W. Adams, M. L. Mielke, M. Garcia-Alloza, K. D. Micheva, S. J. Smith, M. L. Kim, V. M. Lee, B. T. Hyman, T. L. Spires-Jones, *Proc. Natl. Acad. Sci. USA* **2009**, *106*, 4012–4017; d) R. M. Cohen, K. Rezai-Zadeh, T. M. Weitz, A. Rentsendorj, D. Gate, I. Spivak, Y. Bholat, V. Vasilevko, C. G. Glabe, J. J. Breunig, P. Rakic, H. Davtyan, M. G. Agadjanyan, V. Kepe, J. R. Barrio, S. Bannykh, C. A. Szekely, R. N. Pechnick, T. Town, *J. Neurosci.* **2013**, *33*, 6245–6256.

[6] N. Vasdev, P. Cao, E. M. van Oosten, A. A. Wilson, S. Houle, G. Hao, X. Sun, N. Slavine, M. Alhasan, P. P. Antich, F. J. Bonte, P. Kulkarni, *MedChemComm* **2012**, *3*, 1228–1230.

[7] a) M. A. Lovell, J. D. Robertson, W. J. Teesdale, J. L. Campbell, W. R. Markesbery, *J. Neurol. Sci.* **1998**, *158*, 47–52; b) J. H. Viles, *Coord. Chem. Rev.* **2012**, *256*, 2271–2284; c) S. Bolognin, L. Messori, D. Drago, C. Gabbiani, L. Cendron, P. Zatta, *Int. J. Biochem. Cell Biol.* **2011**, *43*, 877–885; d) A. R. White, X. Huang, M. F. Jobling, C. J. Barrow, K. Beyreuther, C. L. Masters, A. I. Bush, R. Cappai, *J. Neurochem.* **2001**, *76*, 1509–1520.

[8] a) R. A. Cherny, J. T. Legg, C. A. McLean, D. P. Fairlie, X. Huang, C. S. Atwood, K. Beyreuther, R. E. Tanzi, C. L. Masters, A. I. Bush, *J. Biol. Chem.* **1999**, *274*, 23223–23228; b) J.-Y. Lee, J. E. Friedman, I. Angel, A. Kozak, J.-Y. Koh, *Neurobiol. Aging* **2004**, *25*, 1315–1321; c) J.-S. Choi, J. J. Braymer, R. P. R. Nanga, A. Ramamoorthy, M. H. Lim, *Proc. Natl. Acad. Sci. USA* **2010**, *107*, 21990–21995; d) B. P. Cary, A. F. Brooks, M. V. Fawaz, X. Shao, T. J. Desmond, G. M. Carpenter, P. Sherman, C. A. Quesada, R. L. Albin, P. J. H. Scott, *ACS Med. Chem. Lett.* **2015**, *6*, 112–116.

[9] S. H. Liang, J. P. Holland, N. A. Stephenson, A. Kassenbrock, B. H. Rotstein, C. P. Daignault, R. Lewis, L. Collier, J. M. Hooker, N. Vasdev, *ACS Chem. Neurosci.* **2015**, *6*, 535–541.

[10] a) J. Fripp, P. Bourgeat, O. Acosta, P. Raniga, M. Modat, K. E. Pike, G. Jones, G. O'Keefe, C. L. Masters, D. Ames, K. A. Ellis, P. Maruff, J. Currie, V. L. Villemagne, C. C. Rowe, O. Salvado, S. Ourselin, *NeuroImage* **2008**, *43*, 430–439; b) A. B. Rodell, G. O'Keefe, C. C. Rowe, V. L. Villemagne, A. Gjedde, *Front. Aging Neurosci.* **2017**, 8; c) G. D. Rabinovici, A. J. Furst, J. P. O'Neil, C. A. Racine, E. C. Mormino, S. L. Baker, S. Chetty, P. Patel, T. A. Pagliaro, W. E. Klunk, C. A. Mathis, H. J. Rosen, B. L. Miller, W. J. Jagust, *Neurology* **2007**, *68*, 1205–1212.

[11] R. A. Cherny, C. S. Atwood, M. E. Xilinas, D. N. Gray, W. D. Jones, C. A. McLean, K. J. Barnham, I. Volitakis, F. W. Fraser, Y.-S. Kim, X. Huang, L. E. Goldstein, R. D. Moir, J. T. Lim, K. Beyreuther, H. Zheng, R. E. Tanzi, C. L. Masters, A. I. Bush, *Neuron* **2001**, *30*, 665–676.

[12] S. R. Bareggi, U. Cornelli, *CNS Neurosci. Ther.* **2012**, *18*, 41–46.

[13] S. H. Liang, T. L. Collier, B. H. Rotstein, R. Lewis, M. Steck, N. Vasdev, *Chem. Commun.* **2013**, *49*, 8755–8757.

[14] M. A. Klenner, B. Zhang, G. Ciancaleoni, J. K. Howard, H. E. Maynard-Casely, J. K. Clegg, M. Massi, B. H. Fraser, G. Pascali, *RSC Adv.* **2020**, *10*, 8853–8865.

[15] a) M. A. Klenner, G. Pascali, B. Zhang, T. R. Sia, L. K. Spare, A. M. Krause-Heuer, J. R. Aldrich-Wright, I. Greguric, A. J. Guastella, M. Massi, B. H. Fraser, *Chem. Eur. J.* **2017**, *23*, 6499–6503; b) M. A. Klenner, G. Pascali, B. Zhang, G. Ciancaleoni, M. Massi, B. H. Fraser, *Aust. J. Chem.* **2019,** *72*, 288–294; c) B. Zhang, B. H. Fraser, M. A. Klenner, Z. Chen, S. H. Liang, M. Massi, A. J. Robinson, G. Pascali, *Chem. Eur. J.* **2019**, *25*, 7613–7617.

[16] G. Pascali, G. Nannavecchia, S. Pitzianti, P. A. Salvadori, *Nucl. Med. Biol.* **2011**, *38*, 637–644.

[17] a) G. Tang, M. Wang, X. Tang, M. Gan, L. Luo, *Nucl. Med. Biol.* **2005**, *32*, 553–558; b) D. Kobus, Y. Giesen, R. Ullrich, H. Backes, B. Neumaier, *Appl. Radiat. Isot.* **2009**, *67*, 1977–1984; c) V. Paolillo, S. Riese, J. G. Gelovani, M. M. Alauddin, *J. Labelled Compd. Radiopharm.* **2009**, *52*, 553–558; d) T. Bourdier, I. Greguric, P. Roselt, T. Jackson, J. Faragalla, A. Katsifis, *Nucl. Med. Biol.* **2011**, *38*, 645–651; e) B. G. Hockley, M. N. Stewart, P. Sherman, C. Quesada, M. R. Kilbourn, R. L. Albin, P. J. H. Scott, *J. Labelled Compd. Radiopharm.* **2013**, *56*, 595–599; f) A. Haslop, A. Gee, C. Plisson, N. Long, *J. Labelled Compd. Radiopharm.* **2013**, *56*, 313–316; g) Y. Liu, L. Zhu, K. Plössl, S. R. Choi, H. Qiao, X. Sun, S. Li, Z. Zha, H. F. Kung, *Nucl. Med. Biol.* **2010**, *37*, 917–925; h) J. Henrottin, C. Lemaire, D. Egrise, A. Zervosen, B. Van den Eynde, A. Plenevaux, X. Franci, S. Goldman, A. Luxen, *Nucl. Med. Biol.* **2016**, *43*, 379–389; i) M. Patt, A. Schildan, B. Habermann, S. Fischer, A. Hiller, W. Deuther-Conrad, S. Wilke, R. Smits, A. Hoepping, G. Wagenknecht, J. Steinbach, P. Brust, O. Sabri, *Appl. Radiat. Isot.* **2013**, *80*, 7–11; j) S. Guillouet, D. Patin, O. Tirel, J. Delamare, F. Gourand, J. B. Deloye, M. Leporrier, L. Barré, *Mol. Imaging Biol.* **2014**, *16*, 28–35; k) B. W. Schoultz, B. J. Reed, J. Marton, F. Willoch, G. Henriksen, *Molecules* **2013**, *18*, 7271–7278; l) S. K. Nandy, M. G. R. Rajan, *Appl. Radiat. Isot.* **2010**, *68*, 1944–1949; m) J. Liu, V. Kepe, A. Žabjek, A. Petrič, H. C. Padgett, N. Satyamurthy, J. R. Barrio, *Mol. Imaging Biol.* **2007**, *9*, 6–16; n) D. Thonon, D. Goblet, E. Goukens, G. Kaisin, J. Paris, J. Aerts, S. Lignon, X. Franci, R. Hustinx, A. Luxen, *Mol. Imaging Biol.* **2011**, *13*, 1088–1095.

[18] A. Philippidis. *Genet. Eng. Biotechn. N.* **2018**, *38*, 6.

[19] a) C.-C. Lee, G. Sui, A. Elizarov, C. J. Shu, Y.-S. Shin, A. N. Dooley, J. Huang, A. Daridon, P. Wyatt, D. Stout, H. C. Kolb, O. N. Witte, N. Satyamurthy, J. R. Heath, M. E. Phelps, S. R. Quake, H.-R. Tseng, *Science* **2005**, *310*, 1793; b) M.-W. Wang, Y.-P. Zhang, Y.-J. Zhang, C. Shen, *J. Radioanal. Nucl. Chem.* **2011**, *289*, 191; c) W. Sun, J. Wilson, P. Kumar, E. Knaus, L. Wiebe, *Curr. Radiopharm.* **2009**, *2*, 75–82; d) O. Jacobson, D. O. Kiesewetter, X. Chen, *Bioconjugate Chem.* **2015**, *26*, 1–18.

[20] a) M. Pahl, M. Mayer, M. Schneider, D. Belder, K. R. Asmis, *Anal. Chem.* **2019**, *91*, 3199–3203; b) P. G. Graham, D. C. Weatherburn, *Aust. J. Chem.* **1981**, *34*, 291–300; c) B. Fecher, H. Elias, *Inorg. Chim. Acta* **1990**, *168*, 179–187; d) P. Ketan, Y. Bernard, R. G. John, I. M. Veronique, L. Wen-Hsuan, A. P. John, B. B. Aaron, F. J. Klavs, *J. Flow Chem.* **2011**, *1*, 53–55.

[21] a) R. Sakla, A. Singh, R. Kaushik, P. Kumar, D. A. Jose, *Inorg. Chem.* **2019**, *58*, 10761–10768; b) S. Pai, M. Hafftlang, G. Atongo, C. Nagel, J. Niesel, S. Botov, H.-G. Schmalz, B. Yard, U. Schatzschneider, *Dalton Trans.* **2014**, *43*, 8664–8678; c) M. J. Stout, A. Stefan, B. W. Skelton, A. N. Sobolev, M. Massi, A. Hochkoeppler, S. Stagni, P. V. Simpson, *Eur. J. Inorg. Chem.* **2020**, *2020*, 292–298; d) N. Rana, H. E. Jesse, M. Tinajero-Trejo, J. A. Butler, J. D. Tarlit, M. L. von Und Zur Muhlen, C. Nagel, U. Schatzschneider, R. K. Poole, *Microbiology* **2017**, *163*, 1477–1489; e) K. Ling, F. Men, W.-C. Wang, Y.-Q. Zhou, H.-W. Zhang, D.-W. Ye, *J. Med. Chem.* **2018**, *61*, 2611–2635; f) H.-M. Berends, P. Kurz, *Inorg. Chim. Acta* **2012**, *380*, 141–147.

[22] D. Ory, J. Van den Brande, T. de Groot, K. Serdons, M. Bex, L. Declercq, F. Cleeren, M. Ooms, K. Van Laere, A. Verbruggen, G. Bormans, *J. Pharm. Biomed. Anal.* **2015**, *111*, 209–214.

Received: May 3, 2020